On pre-emptive vehicle stability control

Taylor & Francis
Taylor & Francis Group

Vehicle System Dynamics

International Journal of Vehicle Mechanics and Mobility

ISSN: (Print) (Online) Journal homepage: www.tandfonline.com/journals/nvsd20

On pre-emptive vehicle stability control

Alberto Parra, Davide Tavernini, Patrick Gruber, Aldo Sorniotti, Asier Zubizarreta & Joshué Pérez

To cite this article: Alberto Parra, Davide Tavernini, Patrick Gruber, Aldo Sorniotti, Asier Zubizarreta & Joshué Pérez (2022) On pre-emptive vehicle stability control, Vehicle System Dynamics, 60:6, 2098-2123, DOI: 10.1080/00423114.2021.1895229

To link to this article: https://doi.org/10.1080/00423114.2021.1895229

Published online: 30 Mar 2021.

VEHICLE SYSTEM DYNAMICS
2022, VOL. 60, NO. 6, 2098–2123
https://doi.org/10.1080/00423114.2021.1895229

On pre-emptive vehicle stability control

Alberto Parra [a,b], Davide Tavernini [c], Patrick Gruber [c], Aldo Sorniotti [c], Asier Zubizarreta [b] and Joshué Pérez [a]

[a]Tecnalia, Basque Research and Technology Alliance (BRTA), Derio, Spain; [b]University of the Basque Country (UPV/EHU), Bilbao, Spain; [c]University of Surrey, Guildford, UK

ABSTRACT

Future vehicle localisation technologies enable major enhancements of vehicle dynamics control. This study proposes a novel vehicle stability control paradigm, based on pre-emptive control that considers the curvature profile of the expected path ahead in the computation of the reference direct yaw moment and braking control action. The additional information allows pre-emptive trail braking control, which slows down the vehicle if the predicted speed profile based on the current torque demand is deemed incompatible with the reference trajectory ahead. Nonlinear model predictive control is used to implement the approach, in which also the steering angle and reference yaw rate provided to the internal model are varied along the prediction horizon, to account for the expected vehicle path. Two pre-emptive stability control configurations with different levels of complexity are proposed and compared with the passive vehicle, and two state-of-the-art nonlinear model predictive stability controllers, one with and one without non-pre-emptive trail braking control. The performance is assessed along obstacle avoidance tests, simulated with a high-fidelity model of an electric vehicle with in-wheel motors. Results show that the pre-emptive controllers achieve higher maximum entry speeds – up to $\sim$34% and $\sim$60% in high and low tyre-road friction conditions – than the formulations without preview.

ARTICLE HISTORY
Received 4 September 2020
Revised 31 January 2021
Accepted 7 February 2021

KEYWORDS
Nonlinear model predictive control; stability control; torque-vectoring; direct yaw moment control; trail braking; pre-emptive control

1. Introduction

Stability control systems were introduced in the 1990s [1], and are based on the feedback control of vehicle yaw rate and sideslip angle, through the application of direct yaw moment control, i.e. a yaw moment generated by the longitudinal force difference between the tyres on the left and right vehicle sides, as well as the application of driver-independent braking actions to slow down the vehicle. At large vehicle sideslip angles the driver loses authority over the cornering response as tyre forces are mostly saturated and steering inputs will not significantly influence the total yaw moment [2]. Vehicle stability controllers prevent this scenario by keeping the sideslip angle within safe thresholds, such that the driver – or the automated driving system – can control the cornering condition through the steering

CONTACT Aldo Sorniotti a.sorniotti@surrey.ac.uk

angle. The effectiveness of vehicle stability control systems in enhancing active safety and reducing road accidents has been widely discussed [3,4].

The vehicle stability control function can be actuated through: (a) the friction brakes, which is the common solution of production passenger cars during emergency conditions, and (b) the individual control of electric powertrains or torque-vectoring (TV) devices, which allows continuous and seamless operation of direct yaw moment control, and can also be used for agility enhancement [5]. Several control structures have been proposed for vehicle stability and agility control through direct yaw moment control, including proportional integral derivative controllers [5], linear quadratic regulators [6], H_∞ controllers [7], sliding mode controllers [8,9], fuzzy logic controllers [10], and model predictive controllers [11–13]. To further enhance active safety, vehicle stability controllers have been extended with additional control functions, on top of the original yaw rate error, sideslip angle, and wheel slip limitation functions. For example, modern systems can include roll-over control [14], control of the hitch angle oscillations when the car tows a trailer [15,16], and trail braking control to manage the balance between longitudinal and lateral dynamics [17].

Although the automotive sector is making significant efforts towards vehicle connectivity functions and driving automation [18], in the near future vehicle stability control systems are expected to remain implemented as separate functions based on feedback control of yaw rate and sideslip angle. The automated driving systems that are progressively introduced on the market tend to keep the vehicle well within its cornering limit, i.e. in its linear operating region, far from the intervention thresholds of stability controllers. Hence, the engineering effort towards driving automation is not likely to bring an immediate major change in vehicle stability control technology. Likewise, the state-of-the-art vehicle stability and torque-vectoring controllers based on model predictive control technology do not yet use their full potential. The recent formulations consider constant steering wheel angle and reference yaw rate along the prediction horizon. Therefore, a relatively long prediction horizon is not very beneficial as the system does not attempt to forecast the vehicle response based on what the driver or automated driving system are likely to do [11–13, 16]. Recent analyses and experimental validations of advanced controllers for automated vehicles operating at the limit of handling investigate the options of: (i) relaxing the typical vehicle stability constraints, e.g. on sideslip angle, to prioritise the tracking of the reference path during automated emergency manoeuvring [19]; and (ii) calculating the direct yaw moment control action with a path tracking objective, rather than for tracking a reference yaw rate and limiting sideslip angle [20–22]. In the context of human-driven vehicles, reference [23] uses the modified Hamiltonian algorithm (MHA) to implement the low level control layer of the so-called advanced emergency cornering (AEC) function, which intervenes through steering control and individual wheel torque control, i.e. by overruling the human commands, to keep the vehicle along the reference path if the driver does not provide the expected inputs.

However, such implementations would need a radical change of the vehicle control architecture – the integration of the path tracking and vehicle stability control functions – which would only be viable for vehicles with high levels of driving automation. In summary, the literature lacks analyses of novel potential stability control options, enabled by the ongoing improvement of localisation technologies, and potentially implementable in relatively short term on a wide range of vehicles, both human-driven and automated.

This paper targets the identified gap by proposing a pre-emptive stability control concept. For example, when appropriate before the entry of a corner, the knowledge of the current position of the ego vehicle, together with the information on the expected path ahead, is used to pre-emptively reduce the speed to a level that allows safe negotiation of the turn. The philosophy remains the one of the stability control paradigm, e.g. the pre-emptive braking action is applied only as a last resort and at the minimum intensity level to ensure safe operation along the expected trajectory, within a specified tolerance with respect to the limit of handling. In the same scenario, a conventional stability controller would allow excessively high entry speeds, yielding a rising yaw rate error and sideslip angle, which will then prompt braking and direct yaw moment control to try to stabilise the vehicle. Because of the physical constraints of tyre-road friction, the delayed stabilising effect could be insufficient to keep the vehicle along its expected path.

Model predictive control (MPC) is well-suited for the development of a pre-emptive controller as it can account for the future expected inputs and references as well as system dynamics in the computation of the optimal control action along a prediction horizon, while formally considering constraints. Given the significant system nonlinearities during the vehicle stability control interventions, implicit nonlinear model predictive control (NMPC) [24,25] is selected for the preliminary implementation of the pre-emptive stability control concept. MPC has been widely demonstrated for pre-emptive automotive controllers, e.g. see its application to a suspension system with road preview in [26]. Other MPC approaches – alternative to the selected NMPC – are linear MPC, which uses a prediction model obtained by linearisation, linear time varying MPC, which recalculates the linear model step-by-step for the current operating condition of the vehicle, and hybrid MPC, which can simplify the lateral tyre force characteristic as a function of slip angle with bilinear functions. These alternative approaches are particularly effective if, within the prediction horizon, the vehicle remains close to the operating point for which the simplified prediction model was designed. This approximation can work relatively well for the typically short prediction horizons of MPC implementations for non-pre-emptive vehicle dynamics and stability control, in which the steering input and the reference yaw rate are considered constant along the prediction horizon, in absence of any further information on the expected path ahead. However, the simplified MPC approaches lead to poor predictions and performance when longer prediction horizons, like those of this study, are considered, and the expected variations of steering angle and reference yaw rate are accounted for in the formulation, which can imply major cornering stiffness variations within the prediction horizon. Although NMPC tends to be more computationally intensive than linear or linear time varying MPC, the computational capabilities of automotive control units have significantly improved, and fast integration-based algorithms are available, which allow to compute the solution within acceptable times, compatible with vehicle implementations.

The pre-emptive stability control function is practically feasible with existing technology, as it requires: (i) vehicle localisation, which is achieved by a global navigation satellite system, possibly improved through fusion with the measurements from other sensors, such as inertial measurement units, LiDARS, radars, and cameras; and (ii) road scenario maps, e.g. available in common navigation systems, for the computation of the expected road curvature ahead.

The contributions of this study are:

- The mathematical formulation of two pre-emptive stability controllers, with different levels of complexity, based on the variation of the total wheel torque demand and generation of a direct yaw moment;
- The comparison of the performance of the pre-emptive vehicle stability controllers with that of state-of-the-art feedback stability controllers based on nonlinear model predictive control during obstacle avoidance tests. The manoeuvres are simulated with a high-fidelity model of a four-wheel-drive electric vehicle with in-wheel motors and torque-vectoring capability.

The remainder of the paper is organised as follows: Section 2 describes the controller configurations; Section 3 discusses the simulation framework; and Section 4 analyses the simulation results, which are used to draw the conclusions in Section 5.

2. Controller configurations

The following subsections provide the details of the nonlinear optimal control problem formulations for the stability control options based on continuous TV actuation that are compared in this study, namely: (i) Baseline TV, abbreviated as Base-TV in the remainder: an NMPC formulation including yaw rate tracking and sideslip angle limitation, in which the steering angle and reference yaw rate remain constant along the prediction horizon [27]; (ii) Trail braking TV (TBrk-TV): the Base-TV controller extended by a trail braking control action, see [17], if the vehicle speed is deemed excessively high with respect to the current curvature radius; (iii) Pre-emptive TV (Pre-TV): a pre-emptive TV formulation, in which the information on the expected curvature of the path ahead along the prediction horizon is computed outside the NMPC, under the hypothesis of zero longitudinal acceleration, and is used by the controller; and (iv) Embedded Pre-emptive TV (ePre–TV): similar controller to the Pre-TV, but the information on the expected curvature of the path ahead is computed inside the NMPC formulation and considers the varying longitudinal vehicle dynamics along the prediction horizon.

While the first two TV controllers are based on those proposed in the literature [17,27], both pre-emptive approaches constitute novel contributions.

2.1. Internal model formulation

The internal (or prediction) NMPC model, i.e. the system of differential equations to obtain the system states, is expressed through the following continuous time formulation:

$$\dot{\boldsymbol{x}}(t) = f(\boldsymbol{x}(t), \boldsymbol{u}(t)) \tag{1}$$

where the state vector $\boldsymbol{x}$ is:

$$\boldsymbol{x} = [V \; S \; \beta \; \dot{\psi} \; \omega_{FL} \; \omega_{FR} \; \omega_{RL} \; \omega_{RR}]^T \tag{2}$$

In (2), V is the vehicle speed, S is the travelled distance, β is the vehicle sideslip angle at the centre of gravity, $\dot{\psi}$ is the yaw rate, and ω_{ij} are the angular speeds of each wheel, with

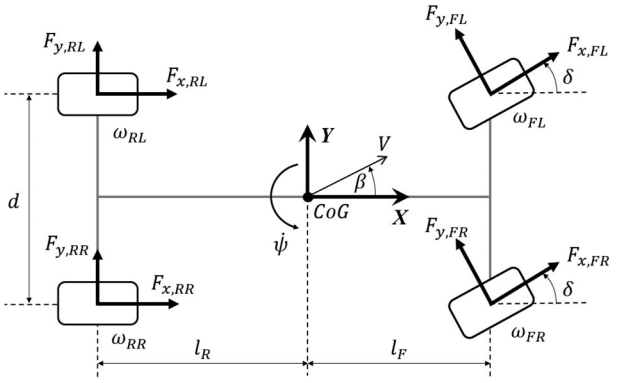

Figure 1. Simplified top view of the vehicle showing the positive directions of the relevant variables.

$i = F, R$ indicating the front or rear axles, and $j = L, R$ indicating the left or right hand sides of the vehicle (see Figure 1). $\boldsymbol{x}$ is also part of the parameter vector, and its current value (obtained from on-board measurements and state estimations) is provided to the controller at each time step, as initial condition for the prediction based on the internal model. The control action is defined as:

$$\boldsymbol{u} = [\tau_L \ \tau_R \ \varepsilon]^T \tag{3}$$

where τ_j are the total wheel torque levels on the left- and right-hand sides of the vehicle, equal to the sum of the individual torques on the respective side; and ε is the slack variable, which allows setting up a soft constraint in the optimal control problem, and is used to limit vehicle speed.

Similarly to recent NMPC implementations for TV [27–29], under the main simplifying assumptions of absence of pitch, roll, heave and unsprung mass dynamics, the prediction model formulation (1) includes 7 degrees of freedom, described by the following force and moment balance equations, see also Figure 1 for the vehicle schematic and nomenclature.

- Longitudinal force balance, i.e. along the direction of the velocity vector at the centre of gravity:

$$\begin{aligned}\dot{V} = \frac{1}{m}\{&[F_{x,FL} + F_{x,FR}]\cos(\delta - \beta) - [F_{y,FL} + F_{y,FR}]\sin(\delta - \beta) \\ &+[F_{x,RL} + F_{x,RR}]\cos\beta + [F_{y,RL} + F_{y,RR}]\sin\beta\}\end{aligned} \tag{4}$$

- Travelled distance equation:

$$\dot{S} = V \tag{5}$$

- Lateral force balance, i.e. along a direction perpendicular to the velocity vector at the centre of gravity:

$$\begin{aligned}\dot{\beta} = \frac{1}{mV}\{&[F_{x,FL} + F_{x,FR}]\sin(\delta - \beta) + [F_{y,FL} + F_{y,FR}]\cos(\delta - \beta) \\ &-[F_{x,RL} + F_{x,RR}]\sin\beta + [F_{y,RL} + F_{y,RR}]\cos\beta\} - \dot{\psi}\end{aligned} \tag{6}$$

- Yaw moment balance:

$$\ddot{\psi} = \frac{1}{I_z}\left\{[F_{x,FL} + F_{x,FR}]l_F \sin\delta + [F_{y,FL} + F_{y,FR}]l_F \cos\delta - [F_{y,RL} + F_{y,RR}]l_R \right.$$
$$\left. + [F_{x,FR}\cos\delta - F_{y,FR}\sin\delta + F_{x,RR}]\frac{d}{2} - [F_{x,FL}\cos\delta - F_{y,FL}\sin\delta + F_{x,RL}]\frac{d}{2}\right\} \tag{7}$$

- *ij* wheel moment balance:

$$\dot{\omega}_{ij} = \frac{\tau_{ij} - F_{x,ij}R_w}{I_\omega} \tag{8}$$

where m is the vehicle mass; I_z is the vehicle yaw moment of inertia; I_ω is the wheel moment of inertia; δ is the steering angle, assumed equal on the two front wheels; $F_{x,ij}$ are the longitudinal tyre forces; $F_{y,ij}$ are the lateral tyre forces; d is the track width; l_F and l_R are the front and rear semi-wheelbases; and R_w is the wheel radius. The computation of S is required only for the pre-emptive formulations; however, given the very limited computational burden associated with this additional state, for uniformity of implementation S was kept also in the non-pre-emptive controllers. The effects of aerodynamic drag and tyre rolling resistance are neglected in (4) and (8).

Within each side, for simplicity the wheel torque levels are distributed according to a constant front-to-total torque distribution ratio, $T_{FtT} = 0.6$ (see [27] for more complex NMPC formulations including advanced wheel torque distributions, which are beyond the scope of this study):

$$\begin{aligned} \tau_{Fj} &= \tau_j T_{FtT} \\ \tau_{Rj} &= \tau_j [1 - T_{FtT}] \end{aligned} \tag{9}$$

where $j = L, R$ indicates the left or right hand sides of the vehicle.

The longitudinal and lateral tyre forces, $F_{x,ij}$ and $F_{y,ij}$, are given by the product of the respective tyre force coefficient, $\mu_{x,ij}$ and $\mu_{y,ij}$, by the vertical tyre load, $F_{z,ij}$:

$$F_{x,ij} = \mu_{x,ij} F_{z,ij} \tag{10}$$

$$F_{y,ij} = \mu_{y,ij} F_{z,ij} \tag{11}$$

A simplified version of the Pacejka Magic Formula [30] determines the total tyre force coefficients, μ_{ij}:

$$\mu_{ij}(s_{ij}) = D\sin(C\,\mathrm{atan}(Bs_{ij})) \tag{12}$$

where B, C and D are Magic Formula constants, calculated to match the actual tyre characteristics of the case study vehicle; and the equivalent slip, s_{ij}, results from the composition of the longitudinal and lateral slip components, $s_{x,ij}$ and $s_{y,ij}$:

$$s_{ij} = \sqrt{s_{x,ij}^2 + s_{y,ij}^2} \tag{13}$$

$s_{x,ij}$ is defined as:

$$s_{x,ij} = \frac{V_{slip,x,ij}}{\omega_{ij} R_w} \tag{14}$$

and $s_{y,ij}$ is given by:

$$s_{y,ij} = \frac{V_{slip,y,ij}}{V_{x,ij}} \tag{15}$$

where the linear slip speeds, $V_{slip,x,ij}$ and $V_{slip,y,ij}$, are calculated as:

$$V_{slip,x,ij} = \omega_{ij} R_w - V_{x,ij} \tag{16}$$

$$V_{slip,y,ij} = -V_{x,ij} \tan \alpha_{ij} \tag{17}$$

where $V_{x,ij}$ is the component of the velocity of the wheel centre in the direction of the longitudinal axis of the tyre reference system. In the calculation of $V_{slip,y,ij}$, simplified linearised expressions are adopted for the tyre slip angles α_{ij} [31]:

$$\begin{aligned} \alpha_{FL} \approx \alpha_{FR} \approx \beta + \frac{\dot{\psi} l_F}{V} - \delta \\ \alpha_{RL} \approx \alpha_{RR} \approx \beta - \frac{\dot{\psi} l_R}{V} \end{aligned} \tag{18}$$

The longitudinal and lateral tyre load coefficients, $\mu_{x,ij}$ and $\mu_{y,ij}$, are obtained by decomposing the total tyre force coefficient from (12), according to the slip components:

$$\mu_{x,ij} = \frac{s_{x,ij}}{s_{ij}} \mu_{ij} \tag{19}$$

$$\mu_{y,ij} = \frac{s_{y,ij}}{s_{ij}} \mu_{ij} \tag{20}$$

The adopted tyre model is a simple yet sufficiently realistic formulation that is easy to tune, and is also independent from the complete set of Magic Formula coefficients of the high-fidelity plant model in Section 3. The feedback nature of NMPC, based on the receding horizon approach, tends to compensate for the inevitable tyre model mismatches, e.g. caused by tyre wear, tyre changes during the vehicle life, and specific road surface properties, which characterise real vehicles.

$F_{z,ij}$ is calculated as the sum of the static load, $F^0_{z,ij}$, longitudinal load transfer, ΔF^x_z, and lateral load transfer, $\Delta F^y_{z,i}$:

$$\begin{aligned} F_{z,FL} &= F^0_{z,FL} - \Delta F^x_z - \Delta F^y_{z,F} \\ F_{z,FR} &= F^0_{z,FR} - \Delta F^x_z + \Delta F^y_{z,F} \\ F_{z,RL} &= F^0_{z,RL} + \Delta F^x_z - \Delta F^y_{z,R} \\ F_{z,RR} &= F^0_{z,RR} + \Delta F^x_z + \Delta F^y_{z,R} \end{aligned} \tag{21}$$

where the static loads are:

$$\begin{aligned} F^0_{z,FL} = F^0_{z,FR} = \frac{1}{2} mg \frac{l_R}{l_F + l_R} \\ F^0_{z,RL} = F^0_{z,RR} = \frac{1}{2} mg \frac{l_F}{l_F + l_R} \end{aligned} \tag{22}$$

and g is the gravitational acceleration. The longitudinal load transfer is given by:

$$\Delta F_z^x = \frac{1}{2}\frac{mha_x}{l_F + l_R} \tag{23}$$

where a_x is the longitudinal acceleration of the vehicle, and h is the centre of gravity height. The front and rear lateral load transfers are:

$$\begin{aligned} \Delta F_{z,F}^y &= \frac{ma_y}{d}\left[\frac{h_{RC}l_R}{l_F + l_R} + \gamma h_{Roll}\right] \\ \Delta F_{z,R}^y &= \frac{ma_y}{d}\left\{\frac{h_{RC}l_F}{l_F + l_R} + [1-\gamma]h_{Roll}\right\} \end{aligned} \tag{24}$$

where h_{RC} is the roll centre height, assumed to be the same for the front and rear suspensions; h_{Roll} is the distance between the centre of gravity and the roll axis; γ is the front-to-total suspension roll stiffness distribution; and a_y is the lateral acceleration of the vehicle. For simplicity, a_x and a_y are assumed constant along the prediction horizon. The effect of this approximation for the relatively long prediction horizons of the pre-emptive formulations will be the subject of future investigations.

2.2. Optimal control problem formulation

The idea of nonlinear model predictive control is to use a simplified model of the plant to predict and optimise the future system behaviour. The control action is obtained by solving, at each sampling instant, a finite horizon optimal control problem, using the current state of the plant. The optimisation yields an optimal control sequence, and the first element in this sequence is applied to the plant, according to the receding horizon approach [24,25].

The proposed NMPC control law minimises the cost function J, subject to appropriate equality and inequality constraints. The optimal control problem is defined in discrete time as:

$$\begin{aligned} &\min_{\boldsymbol{u}} J(\boldsymbol{x}(0), \boldsymbol{u}(\cdot)) := \ell_N(\boldsymbol{x}(N)) + \sum_{k=0}^{N-1} \ell(\boldsymbol{x}(k), \boldsymbol{u}(k)) \\ &\text{s.t.} \\ &\boldsymbol{x}(0) = \boldsymbol{x_{in}} \\ &\boldsymbol{x}(k+1) = f_d(\boldsymbol{x}(k), \boldsymbol{u}(k)) \\ &\underline{\boldsymbol{x}} \le \boldsymbol{x}(k) \le \bar{\boldsymbol{x}} \\ &\underline{\boldsymbol{x}} \le \boldsymbol{x}(N) \le \bar{\boldsymbol{x}} \\ &\underline{\boldsymbol{u}} \le \boldsymbol{u}(k) \le \bar{\boldsymbol{u}} \\ &\boldsymbol{u}(\cdot) : [0, N-1] \end{aligned} \tag{25}$$

where the notation $\boldsymbol{u}(\cdot)$ indicates the control sequence; $\boldsymbol{x_{in}}$ is the initial value of the state vector, obtained from the sensor measurements and state estimators; N is the number of steps of the prediction horizon H_P, in this implementation equal to the control horizon H_c, i.e. $H_c = H_p = NT_s$, with T_s being the discretization time; k indicates the discretization

step along the prediction horizon; $\underline{\boldsymbol{x}}$ and $\bar{\boldsymbol{x}}$ are the lower and upper limits for $\boldsymbol{x}$; $\underline{\boldsymbol{u}}$ and $\bar{\boldsymbol{u}}$ are the lower and upper limits for $\boldsymbol{u}$; $\boldsymbol{x}(k+1) = f_d(\boldsymbol{x}(k), \boldsymbol{u}(k))$ is the discretized version of the model defined in (1), detailed in the previous subsection; $\ell(\boldsymbol{x}(k), \boldsymbol{u}(k))$is the stage cost function associated to each time step, defined as a least-squares function; and $\ell_N(\boldsymbol{x}(N))$ is the terminal cost. For $k = 0$ the variables are measured/estimated, while for $k > 0$ the variables are predicted. As the specific emphasis of this proof-of-concept is on the vehicle dynamics functionality, no formal stability analysis is presented. Nevertheless, the proposed NMPC approach includes a terminal cost, $\ell_N(\boldsymbol{x}(N))$, which forces the system to converge to the desired final state, and enhances stability.

Although the four NMPC implementations share the same internal model, discussed in Section 2.A, they present differences in the definition of the stage cost, the constraints, or the particular behaviour of some variables in the prediction horizon. These differences will be detailed in the following subsections.

Baseline TV (Base-TV)
For the Base-TV, the stage cost formulation is:

$$\ell(\boldsymbol{x}(k), \boldsymbol{u}(k)) = W_{u,F_x}\left\{F_{x,ref}(k) - \frac{1}{R_w}[\tau_L(k) + \tau_R(k)]\right\}^2 + W_{u,\dot{\psi}}[\dot{\psi}_{ref}(k) - \dot{\psi}(k)]^2 + W_{u,\alpha_R}\alpha_R(k)^2 \tag{26}$$

while the terminal cost is:

$$\ell_N(\boldsymbol{x}(N)) = W_{u,\dot{\psi}(N)}[\dot{\psi}_{ref}(N) - \dot{\psi}(N)]^2 \tag{27}$$

where $F_{x,ref}$ is the total force demand from the drivability controller, i.e. the respective cost function term tracks the driver input on the accelerator and (where applicable) brake pedals; $\dot{\psi}_{ref}$ is the reference yaw rate; α_R is the rear axle sideslip angle, which is penalised to enhance stability; and W_{u,F_x}, $W_{u,\dot{\psi}}$, and W_{u,α_R} are the cost function weights, respectively prioritising longitudinal force tracking, reference yaw rate tracking, and rear axle slip angle reduction. In this preliminary proof-of-concept analysis of pre-emptive stability control, ℓ is purposely simple; however, it could include additional terms, e.g. to reduce energy consumption, as proposed in [27], or to prevent roll-over [11]. The consideration of α_R, which is calculated through (18), ensures vehicle stability and avoids oversteer, which could be the result of extreme transient conditions. Only the rear axle sideslip angle is explicitly considered in the cost function, while the reduction of vehicle understeer, which tends to occur less abruptly than oversteer and is associated with the front slip angle, is implicitly addressed by the yaw rate tracking term. As a matter of fact, nearly all production vehicles tend to be understeering rather than oversteering, as understeer is usually considered more controllable by the driver and less dangerous than oversteer.

In the Base-TV formulation, the steering input used in the internal model, as well as the reference yaw rate in the cost function, are kept constant along the prediction horizon, and equal to their current value [27]:

$$\delta(k) = \delta(0) \tag{28}$$

$$\dot{\psi}_{ref}(k) = \frac{V(0)}{l_F + l_R + V(0)^2 K_{US}}\delta(0) \tag{29}$$

where (29) derives from the well-known single-track model, and K_{US} is the understeer coefficient [32], which was selected to be aligned with the one of the vehicle without control, in its linear operating region.

The following constraints have been implemented in (25) as box constraints, i.e. defining lower and upper limits:

- Yaw rate constraint, fixed along the prediction horizon, i.e. $|\dot{\psi}(k)| \leq a_{y,\max}/V(0) = F_s\hat{\mu}_{\max}(0)g/V(0)$, where $a_{y,\max}$ is the maximum possible lateral acceleration of the vehicle; $\hat{\mu}_{\max}(0)$ is the current estimated value of the tyre-road friction coefficient, which on a real vehicle would be output by a state estimator, and in the preliminary analysis of this study is assumed to be known; and $F_s \leq 1$ is a safety factor, providing conservativeness to the controller performance.
- Sideslip angle constraint, i.e. $|\beta| \leq \beta_{\max}(0)$, set to 5 deg for the simulations of this study.
- Individual tyre slip ratio constraints, i.e. $|s_{x,ij}| \leq s_{x,\max,ij}(0)$, where $s_{x,\max,ij}$ is the maximum allowed value of longitudinal slip, set to 0.15.
- Individual wheel torque constraints, i.e. $|\tau_{ij}| \leq \tau_{\max,ij}(0)$, where $\tau_{\max,ij}$ is the maximum powertrain torque at the current vehicle speed. The specific obstacle avoidance tests of this preliminary study did not require the intervention of the friction brakes. Appropriate additional formulations, which are beyond the scope of this paper, would be needed for the torque blending between electric powertrains and friction brakes.

Trail Braking TV (TBrk-TV)

With respect to the TV-Base, the stage cost of the TBrk-TV case also includes a term penalising the slack variable ε:

$$\ell(\boldsymbol{x}(k), \boldsymbol{u}(k)) = W_{u,F_x}\left\{F_{x,ref}(k) - \frac{1}{R_w}[\tau_L(k) + \tau_R(k)]\right\}^2 + W_{u,\dot{\psi}}[\dot{\psi}_{ref}(k) - \dot{\psi}(k)]^2 + W_{u,\alpha_R}\alpha_R(k)^2 + W_{u,\varepsilon}\varepsilon(k)^2 \tag{30}$$

ε is used to define a soft constraint on vehicle speed:

$$V(k) < V_{\max}(0) + \varepsilon(k), \text{ with } \varepsilon \geq 0 \tag{31}$$

where $V_{\max}(0)$ is estimated at the beginning of the prediction horizon, i.e. without considering the expected path ahead [17]:

$$V_{\max}(0) = \frac{a_{y,\max}}{\dot{\psi}(0)} = \frac{F_s\hat{\mu}_{\max}(0)g}{\dot{\psi}(0)} \tag{32}$$

$\dot{\psi}(0)$ is the vehicle yaw rate, measured by the on-board sensor. The conditions in (30)–(32) ensure that the speed is compatible with the current cornering condition, by slowing down the vehicle through a wheel torque reduction, if required. The trail braking functionality of the TBrk-TV configuration, see [17], is already beyond the standard capabilities of conventional vehicle stability controllers. A soft constraint on vehicle speed, V, is used rather than a hard constraint, i.e. $V(k) < V_{\max}(0)$, as the latter may lead to infeasibilities in the solution of the nonlinear optimal control problem. The slack variable, ε, implements the soft constraint. In the ideal case, ε is zero and (31) turns into a hard constraint. However,

if the solver cannot compute a solution, the slack variable can take a value that allows fulfilling the constraint in a 'soft' way through the term $W_{u,\varepsilon}\varepsilon(k)^2$ in (30), which penalises ε, and tries to set its value as close as possible to zero, but also allows some flexibility to facilitate the numerical process.

Pre-emptive TV (Pre-TV)
In the Pre-TV formulation, ℓ is the same as for the TBrk-TV case. However, the implementation differs from the TBrk-TV one as:

- The reference yaw rate varies along the prediction horizon, according the estimated variation of the reference trajectory radius, $R_{ref}(k)$, whose calculation is detailed below (see also Figure 2), under the assumptions of constant vehicle speed, equal to $V(0)$, and negligible sideslip rate [32]:

$$\dot{\psi}_{ref}(k) = \frac{V(0)}{R_{ref}(k)} \tag{33}$$

- The steering angle provided to the internal model varies along the prediction horizon according to the following formulation, based on the sum of the predicted kinematic (or Ackerman) and dynamic steering angle contributions, where the latter is calculated from the understeer coefficient, K_{US}, and the predicted lateral acceleration profile, $a_y^*(k)$ [33]:

$$\delta(k) = \delta_{kin}(k) + \delta_{dyn}(k) \tag{34}$$

$$\delta_{kin}(k) \approx \tan^{-1}\frac{l}{R_{ref}(k)} \tag{35}$$

$$\delta_{dyn}(k) = K_{US}a_y^*(k) \approx \frac{K_{US}V(0)^2}{R_{ref}(k)} \tag{36}$$

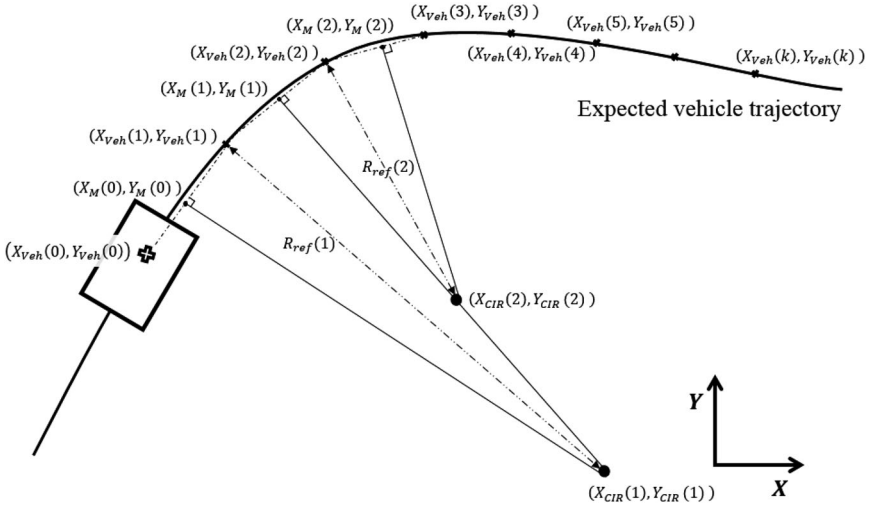

Figure 2. Example of reference trajectory radius calculation for the first two prediction steps.

- The soft constraint on the longitudinal vehicle speed, used by the trail braking function, is based on a varying $V_{\max}$, expressed as a function of the maximum safe lateral acceleration, $a_{y,\max}(0)$, and $R_{ref}(k)$:

$$\begin{aligned} V(k) &< V_{\max}(k) + \varepsilon(k) \\ V_{\max}(k) &= \sqrt{a_{y,\max}(0) R_{ref}(k)} \end{aligned} \tag{37}$$

In the Pre-TV, the sequence of $R_{ref}(k)$ values along the prediction horizon in (34)-(37) is provided to the NMPC as part of the parameter vector by an external function, which, under the assumption of constant vehicle speed, carries out analytical calculations corresponding to the geometric representation in Figure 2. The continuous line in the figure is the expected vehicle trajectory. For each controller run, the algorithm generates a piecewise linear approximation of the curved trajectory, through segments connecting the expected positions of the vehicle at the discrete time values along the prediction horizon, i.e. the start point of each segment has coordinates $(X_{Veh}(k-1), Y_{Veh}(k-1))$, while the end point is defined by $(X_{Veh}(k), Y_{Veh}(k))$. The instantaneous centre of rotation at the time step k, with coordinates $(X_{CIR}(k), Y_{CIR}(k))$, is obtained as the intersection point of the lines perpendicular to two adjacent segments of the linear piecewise approximation of the reference trajectory, each of them drawn from the middle points, $(X_M(k-1), Y_M(k-1))$ and $(X_M(k), Y_M(k))$, of the respective segment:

$$X_{CIR}(k) = \frac{Y_0(k) - Y_0(k-1)}{M_p(k-1) - M_p(k)} \tag{38}$$

$$Y_{CIR}(k) = M_p(k) X_{CIR}(k) + Y_0(k) \tag{39}$$

where $M_p(k)$ and $M_p(k-1)$ are the slopes of the lines perpendicular to the segments connecting the expected vehicle positions at the relevant adjacent times. $M_p(k)$ is given by:

$$M_p(k) = -\frac{1}{M(k)} = -\frac{X_{Veh}(k+1) - X_{Veh}(k)}{Y_{Veh}(k+1) - Y_{Veh}(k)} \tag{40}$$

where $M(k)$ is the slope of the segment connecting the expected vehicle positions at $k-1$ and k. $Y_0(k)$ and $Y_0(k-1)$ are the intersection points of the same lines, passing through the middle points of the segments, with the Y axis of the inertial reference system; for example, $Y_0(k)$ is computed as:

$$Y_0(k) = Y_M(k) - M_p(k) X_M(k) \tag{41}$$

where $X_M(k)$ and $Y_M(k)$ are:

$$X_M(k) = \frac{X_{Veh}(k) + X_{Veh}(k+1)}{2} \tag{42}$$

$$Y_M(k) = \frac{Y_{Veh}(k) + Y_{Veh}(k+1)}{2} \tag{43}$$

The reference trajectory radius at the prediction step k, $R_{ref}(k)$, is the distance between the centre of instantaneous rotation and the expected vehicle position at k:

$$R_{ref}(k) = \sqrt{[X_{CIR}(k) - X_{Veh}(k)]^2 + [Y_{CIR}(k) - Y_{Veh}(k)]^2} \tag{44}$$

At each iteration this process is carried out along the entire target trajectory within the prediction horizon.

Embedded Pre-emptive TV (ePre-TV)
The ePre-TV implementation differs from the Pre-TV as the required trajectory-related variables are computed by considering the vehicle speed variation predicted by the internal model along the prediction horizon, according to (4), i.e. the reference yaw rate formulation becomes:

$$\dot{\psi}_{ref}(k) = \frac{V(k)}{R_{ref,app}(k)} \tag{45}$$

while the dynamic steering angle is given by:

$$\delta_{dyn}(k) = K_{US} a_y^*(k) = \frac{K_{US} V(k)^2}{R_{ref,app}(k)} \tag{46}$$

where $R_{ref,app}(k)$ is the approximated reference turning radius. In the Pre-TV case, $R_{ref,app}(k)$ is computed within the NMPC by considering the vehicle speed predicted by the internal model, which, differently from the Pre-TV case, varies along the prediction horizon, and thus requires a different calculation method of the reference trajectory radius, embedded in the NMPC. $R_{ref,app}(k)$ is given by the inverse of the reference curvature profile, σ_{ref}, as a function of the distance, $S(k)$, covered by the vehicle along the prediction horizon. In the proof-of-concept set-up of this study, $\sigma_{ref}(S)$ is expressed by a sixth-order polynomial, with coefficients computed by a least-squares function, external to the NMPC, to match the curvature of the reference path along a marginally longer distance than the one that is expected to be covered during the prediction horizon. These coefficients are part of the NMPC parameter vector, and are updated at the implementation frequency of the controller. Hence, $R_{ref,app}(k)$ is given by:

$$\begin{aligned} R_{ref,app}(k) &= \frac{1}{\sigma_{ref}(k)} \\ &= \frac{1}{p_0 + p_1 S(k) + p_2 S(k)^2 + p_3 S(k)^3 + p_4 S(k)^4 + p_5 S(k)^5 + p_6 S(k)^6} \end{aligned} \tag{47}$$

3. Simulation set-up

3.1. Simulation framework

The adopted high-fidelity vehicle dynamics simulation tool is Dynacar, which was developed by Tecnalia and experimentally validated on multiple vehicles [34,35]. The model, which is completely different in its formulation from the prediction model in Section 2 and thus allows reliable control assessment, includes the degrees of freedom of the sprung and unsprung masses, and considers suspension kinematics and dynamics. The multibody approach is based on [36], using one coordinate for each degree of freedom through macro-joints, which leads to high computational efficiency. The tyre forces are modelled with the Magic Formula, version 2006 [30]. Examples of experimental validation of the Dynacar model are provided in [37].

Table 1. Main vehicle parameters.

Symbol	Description and unit	Value
m	Vehicle mass (kg)	649
R_w	Wheel radius (m)	0.26
h	Centre of gravity (CoG) height (m)	0.4
d	Track width	1.33
l_F	Distance from front axle to CoG (m)	0.99
l_R	Distance from rear axle to CoG (m)	0.825
I_x	Roll mass moment of inertia (kg m^2)	200
I_y	Pitch mass moment of inertia (kg m^2)	300
I_z	Yaw mass moment of inertia (kg m^2)	400
$\lvert\tau_{\max}\rvert$	Maximum torque of individual S400 machine (Nm)	400

The case study vehicle is the four-wheel-drive variant of a lightweight electric vehicle with in-wheel direct drive powertrains, developed within the European Horizon 2020 STEVE project, see Table 1 and [27]. The specific powertrain configuration makes the individual wheel torque control particularly effective, thanks to the high bandwidth dynamics of the S400 in-wheel machines, provided by Elaphe Propulsion Technologies.

In addition to the Dynacar vehicle model, the simulation framework, shown in Figure 3, consists of:

- The road scenario module, which defines the geometric and tyre-road friction characteristics of the simulated scenario. In this preliminary assessment, the tyre-road friction coefficient is assumed to be exactly known and used by the controllers as a constant value over the manoeuvre and prediction horizon.
- The virtual driver model of the Dynacar simulation package, based on the linear time-varying model predictive control (LTV MPC) approach in [38], which tracks the reference path, and generates the steering angle δ, accelerator pedal position ρ_a, and brake pedal input ρ_b;
- The drivability layer, which converts the driver inputs on the accelerator and brake pedals into the total longitudinal force demand, $F_{x,ref}$;
- The environment detection module, which generates the vector of the reference trajectory radii for the Pre-TV configuration, and the coefficients, $p_0, \ldots, p_6$, of the polynomial approximating the expected curvature ahead for the ePre-TV case;
- The NMPC TV module, according to the options described in Section 2.

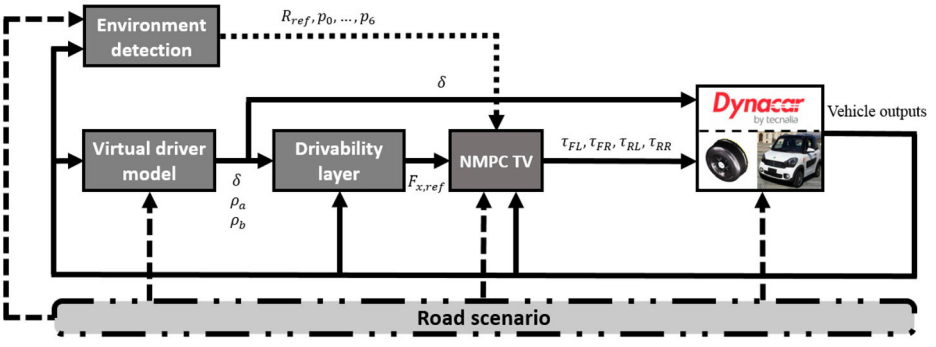

Figure 3. Simplified diagram of the simulation framework.

3.2. Simulated scenarios

The controllers are compared along obstacle avoidance tests, simulated according to the standard ISO3888-2 [39]. The vehicle has to follow a pre-defined course, limited by cones, according to which the vehicle starts in an initial lane, then changes lane to emulate the avoidance of a sudden obstacle, and finally returns into a lane that is offset from the initial one. If the vehicle completes the manoeuvre without hitting a cone, the test is considered successful. The maximum entry speed at which the test is successfully completed provides an indication of the vehicle stability and agility performance.

For an objective comparison, the Dynacar driver model with constant settings is used to control the steering wheel input to follow the reference trajectory. The accelerator pedal is kept in released position throughout the relevant part of the test. To assess the benefit of the pre-emptive controllers, which should slow down the vehicle before entering the obstacle avoidance course, in the simulated scenario the accelerator pedal is released 40 m in front the standard course. This gives sufficient time to the pre-emptive controllers to apply the predictive trail braking control action.

The following simulations compare different configurations of the same vehicle demonstrator, namely the passive set-up (Passive), i.e. the vehicle with the same wheel torque values on the left- and right-hand sides, and constant front-to-total wheel torque distribution within each side; and the vehicle with the Base–TV, TBrk–TV, Pre-TV, and ePre–TV controllers.

For fairness of comparison, all controllers are run with the same nominal settings, i.e. the implementation time is 0.025 s, the time step of the NMPC internal model is 0.025 s, the number of prediction steps is $N = 40$, which corresponds to a prediction horizon of 1 s, longer than for typical non-pre-emptive model predictive vehicle dynamics controllers, such as the one in [27]. The detailed analysis of the effect of H_p and T_s on the performance of the Base-TV is presented in [27], i.e. longer H_p and shorter T_s tend to improve performance, at the price of increased computational effort. Therefore, for completeness, on top of the controllers with the previous nominal values of H_p and T_s, the tables of Section 4 also show the results for: (a) a second Base-TV tuning, referred to as Base-TV2, with the same calibration values as Base-TV, including $N = 40$, but running at 10 ms with $T_s = 10$ ms, and therefore $H_p = 400$ ms; (b) a second Pre-TV tuning, referred to as Pre-TV2, running at 10 ms with the same calibration values as Pre-TV, apart from $T_s = 10$ ms and $N = 100$, and therefore $H_p = 1$ s; and (c) a third Pre-TV tuning, referred to as Pre-TV3, which has been implemented in real-time on a Xilinx Zynq UltraScale+ MPSoC ZCU102 evaluation board, using an ARM Cortex-A53 microcontroller with a clock frequency of 1000 MHz. In this case, the controller is implemented at 50 ms, which corresponds to an average execution time of 22.32 ms. The other calibration parameters are the same as for Pre-TV, and in particular T_s and N are kept equal to 25 ms and 40. The specific real-time code of Pre-TV3 was not subject to any optimisation, which provides confidence on the fact that it could run in real time at lower implementation times and time steps. The apparently rather high time steps and implementation times are not an issue for the specific application, as the yaw and sideslip dynamics of the vehicle are relatively slow.

The controllers are set up through the ACADO toolkit [40], which uses Gauss–Newton iteration algorithms for fast NMPC with constraints, generating locally optimal solutions [41]. The selected solver parameters are: multiple shooting discretization method, fourth order Runge Kutta integrator, and qpOASES QP optimisation algorithm.

3.3. Performance indicators

Objective performance indicators are used to assess the performance of the vehicle configurations along the manoeuvres, namely:

- V_{crit}, i.e. the critical speed, which is the maximum entry speed – the higher the better – at which the considered vehicle configuration manages to successfully complete the obstacle avoidance. In this study, such speed is taken 20 m in advance of the standard obstacle avoidance course, to consider the effect of the predictive trail braking control actions;
- V_{fin}, i.e. the final speed at the exit point of the obstacle avoidance course. A good tuning of the controller should slow down the vehicle as little as possible;
- $RMS(e_{\dot{\psi}})$, i.e. the root mean square value (RMS) of the yaw rate error $e_{\dot{\psi}}$, which assesses the yaw rate tracking performance:

$$RMS(e_{\dot{\psi}}) = \sqrt{\frac{1}{T_{fin} - T_{in}} \int_{T_{in}}^{T_{fin}} [\dot{\psi}_{ref} - \dot{\psi}]^2 dt} \tag{48}$$

  where T_{in} and T_{fin} are the initial and final times of the relevant part of the test, corresponding to the condition of the vehicle entering and exiting the obstacle avoidance course, and t is time;
- $|\alpha_{R,max}|$, i.e. the maximum absolute value of the rear axle sideslip angle during the test, which is an indicator of the level of vehicle stability;
- $IA_{\delta_{SW}}$, i.e. the normalised integral of the absolute value of the steering wheel angle δ_{SW}, which assesses the steering effort made by the virtual driver model to follow the desired path:

$$IA_{\delta_{SW}} = \frac{1}{T_{fin} - T_{in}} \int_{T_{in}}^{T_{fin}} |\delta_{SW}| dt \tag{49}$$

- $IA_{\Delta\delta_{SW}}$, i.e. the normalised integral of the absolute value of the steering wheel rate $\dot{\delta}_{SW} = d\delta_{SW}/dt$, which also assesses the level of steering effort:

$$IA_{\Delta\delta_{SW}} = \frac{1}{T_{fin} - T_{in}} \int_{T_{in}}^{T_{fin}} |\dot{\delta}_{SW}| dt \tag{50}$$

- $IA_{\Delta F_x}$, i.e. the integral of the absolute value of the longitudinal tyre force difference among the two vehicle sides, which assesses the intensity of the direct yaw moment control effort:

$$\begin{aligned} IA_{\Delta F_x} &= \frac{1}{T_{fin} - T_{in}} \int_{T_{in}}^{T_{fin}} |F_{x,FL} - F_{x,FR} + F_{x,RL} - F_{x,RR}| dt \\ &\approx \frac{1}{R_w(T_{fin} - T_{in})} \int_{T_{in}}^{T_{fin}} |\tau_L - \tau_R| dt \end{aligned} \tag{51}$$

  where, in the computation of the indicator, the left and right tyre forces are approximated as the ratios of the side wheel torque, output by the controller, to the wheel radius;

- $IA_{F_{x,tot}}$, i.e. the normalised integral of the absolute value of the longitudinal tyre force reduction imposed by the controller, which provides an indication of the trail braking control effort:

$$IA_{F_{x,tot}} = \frac{1}{T_{fin} - T_{in}} \int_{T_{in}}^{T_{fin}} |F_{x,ref} - [F_{x,FL} + F_{x,FR} + F_{x,RL} + F_{x,RR}]| dt$$
$$\approx \frac{1}{T_{fin} - T_{in}} \int_{T_{in}}^{T_{fin}} \left| F_{x,ref} - \frac{1}{R_w}[\tau_L + \tau_R] \right| dt \quad (52)$$

4. Results

4.1. Obstacle avoidance in high tyre-road friction conditions

Table 2 reports the values of the performance indicators for the considered vehicle configurations along the obstacle avoidance test, for a tyre-road friction parameter equal to 1, at the critical vehicle speed of each controller. Compared to the Passive configuration, V_{crit} of the Base-TV and Base-TV2 controlled vehicles increases respectively by 3 and 5.5 km/h to 56.7 and 59.2 km/h, indicating their enhanced cornering capabilities. This V_{crit} increase is similar to findings reported in other studies [42]. The comparison of Base-TV and Base-TV2 suggests that the reduction of T_s is more effective than the increase of H_P for the specific tuning of the non-pre-emptive controller. Nevertheless, this difference among the Baseline TV tunings does not change the balance of the comparison, and all the other performance indicators are rather aligned for the two Baseline TV configurations; therefore, the following analyses will focus on Base–TV. The trail braking control action of TBrk-TV raises the critical speed to 62 km/h, by slowing down the vehicle, when appropriate, based on the current cornering conditions. The pre–emptive formulations show that a major enhancement in safety performance is achievable through predictive trail braking control. In fact, both pre-emptive controllers with the nominal T_s and H_P manage critical speed values well above 70 km/h, i.e. 73.5 km/h for Pre-TV and 76.0 km/h for ePre-TV. The comparison of Pre-TV, Pre-TV2 and Pre-TV3 highlights that the performance of the pre-emptive controller is rather independent from the implementation step and internal model time step, for the same prediction horizon. For example, the critical speed is the same for Pre-TV3 and Pre–TV, while it is less than 1 km/h higher for Pre-TV2.

Figure 4 plots the reference and actual trajectories during the tests, with the top view of the vehicle reported every 250 ms, while Figure 5 shows the profiles of the main relevant

Table 2. Key performance indicators along the obstacle avoidance tests in high tyre-road friction conditions, carried out from the critical speed for the respective vehicle configuration.

	Passive	Base-TV	Base-TV2	TBrk-TV	Pre-TV	Pre-TV2	Pre-TV3	ePre-TV
V_{crit} (km/h)	53.7	56.7	59.2	62.6	73.5	74.2	73.5	76.0
V_{fin} (km/h)	44.4	45.2	45.8	45.1	44.3	44.9	44.1	42.9
$RMS(e_{\dot{\psi}})$ (deg/s)	5.1	3.8	2.9	2.9	2.0	1.9	2.3	2.2
$\lvert\alpha_{R,\max}\rvert$ (deg)	4.6	3.1	4.0	3.7	2.7	2.8	3.6	2.2
$IA_{\delta_{SW}}$ (deg)	30.7	50.7	49.7	35.6	39.9	33.6	32.8	41.2
$IA_{\Delta\delta_{SW}}$ (deg/s)	143	156	139	130	134	118	126	132
$IA_{\Delta F_x}$ (N)	0	1016	1185	611	592	641	605	681
$IA_{F_{x\,tot}}$ (N)	0	0	0	186	507	544	519	608

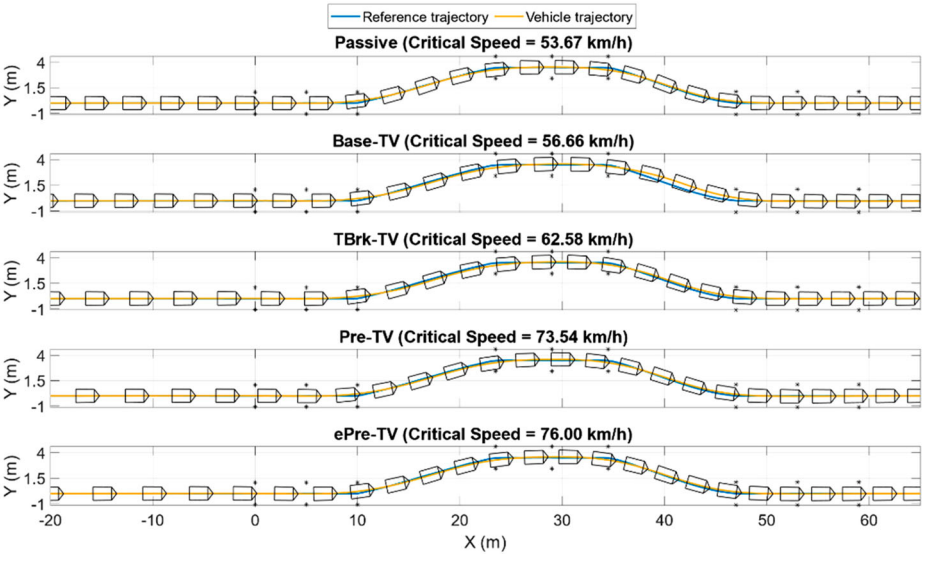

Figure 4. Trajectories along the obstacle avoidance tests in high tyre-road friction conditions, carried out from the critical speed for the respective vehicle configuration.

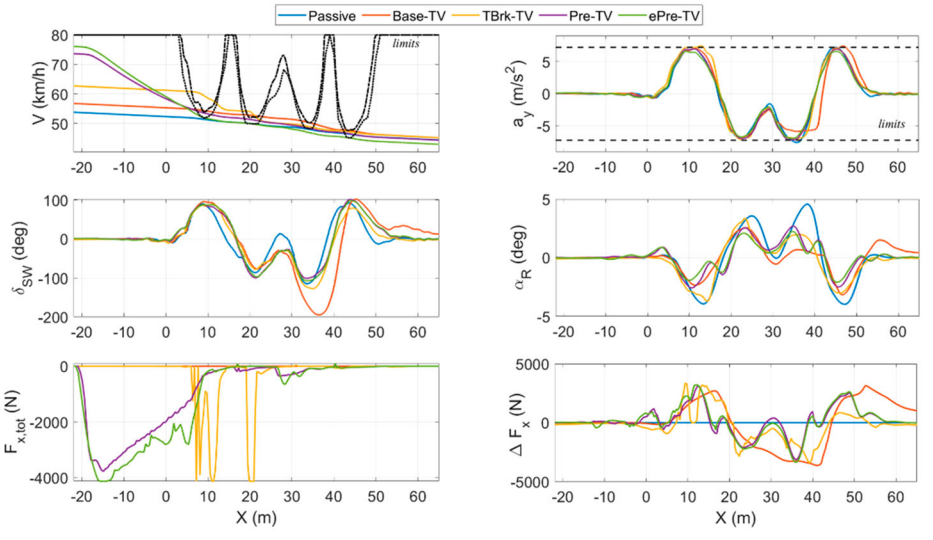

Figure 5. Speed, lateral acceleration, steering wheel angle, rear axle sideslip angle, total longitudinal force ($F_{x,tot} = [\tau_L + \tau_R]/R_w$) and left-to-right longitudinal force difference ($\Delta F_x = [\tau_L - \tau_R]/R_w$) profiles along the obstacle avoidance tests in high tyre-road friction conditions, carried out from the critical speed for the respective vehicle configuration. The black dash-dotted and dotted lines in the speed subplot represent the $V_{\max}$ profiles for Pre-TV and ePre-TV.

variables. In the figures, X and Y represent the vehicle coordinates in the inertial reference frame, with the X axis parallel to the initial lane, and the origin located in the initial point of the expected vehicle trajectory according to the obstacle avoidance course defined by the ISO standard, i.e. $X = 0$ is aligned with the first cone.

In the first three configurations, the vehicle coasts before entering the standard obstacle avoidance course (hence, the spacing among the vehicle representations in Figure 4 is approximately constant in the initial phase of the test), and significantly slows down only after the steering input is applied. In the Passive and Base-TV configurations, the vehicle speed reduction is mainly caused by the lateral tyre slip power losses, and amounts to ~ 10 km/h, as shown by the difference between V_{crit} and V_{fin} in Table 2. TBrk-TV is characterised by the additional trail braking contribution, which intervenes in the sections of the course with tight turning radii, see the rather abrupt braking actions at $X \approx 10$ m and $X \approx 20$ m, and results in an overall ~ 17 km/h vehicle speed reduction. The pre-emptive formulations clearly anticipate the trail braking control action by applying a negative torque starting from $X \approx -20$ m (see the longitudinal speed subplot in Figure 5) to reduce speed to a similar level to that of the Base–TV configuration at the entrance of the manoeuvre. The final vehicle speed is rather similar among all configurations, as it mainly depends on the tyre-road friction limits. Figure 5 also includes the $V_{\max}$ profiles of the pre-emptive formulations, which slightly differ from each other because of the respective approximations in the online computation of the expected trajectory, as well as the marginal difference in the actual vehicle speeds.

The steering effort, evaluated through $IA_{\delta_{SW}}$ and $IA_{\Delta\delta_{SW}}$ in Table 2 and the steering angle profile in Figure 5, is rather similar for all configurations, with the exception of Base-TV, which is affected by significant understeer for $30\,\text{m} \leq X \leq 40\,\text{m}$. $|\alpha_{R,\max}|$ and the rear sideslip angle profiles in Figure 5 show that the stability performance is rather weak for the Passive set-up and, to some extent, the TBrk-TV, which is characterised by larger sideslip values for $10\,\text{m} \leq X \leq 14\,\text{m}$ with respect to the other controlled cases. Such response is caused by the excessive speed of the TBrk-TV vehicle, which applies the trail braking control action only when the actual turning radius becomes tight. In general, the values of $RMS(e_{\dot{\psi}})$ and $|\alpha_{R,\max}|$ as well as the time histories in Figure 5 confirm that TV contributes to vehicle agility and stabilisation throughout the manoeuvre. The considered controllers are characterised by a safety margin with respect to the vehicle cornering limit defined by the available tyre-road friction level, through the factor F_s, which makes the cornering performance rather conservative.

In terms of control effort, the trail braking contribution tends to significantly reduce (by more than 40%) the direct yaw moment control effort, i.e. to lower the difference between left and right powertrain torques, measured by ΔF_x, while, conversely, the values of $IA_{F_{xtot}}$ tend to increase with the level of sophistication of the pre-emptive formulation, see Table 2 and the two bottom plots of Figure 5.

In conclusion, from Figures 4 and 5 and Table 2 it can be inferred that: (i) the pre-emptive trail braking function has higher impact on the maximum initial speed at which the obstacle avoidance manoeuvre can be successfully performed, than the direct yaw moment control action. This important result is a confirmation of the potential significance of the proposed extension of the vehicle stability control concept; and (ii) although the cornering behaviour of the different configurations is rather similar, the main indicators tend to be better for the most advanced controllers.

Figure 6 shows the central processing unit (CPU) time profiles during the execution of the proposed NMPC formulations, running on a computer with an Intel Core i7-6820HQ 2.70 GHz processor and 32 GB RAM. The profiles highlight the most demanding sections of the manoeuvre for each controller. For example, with the pre-emptive configurations,

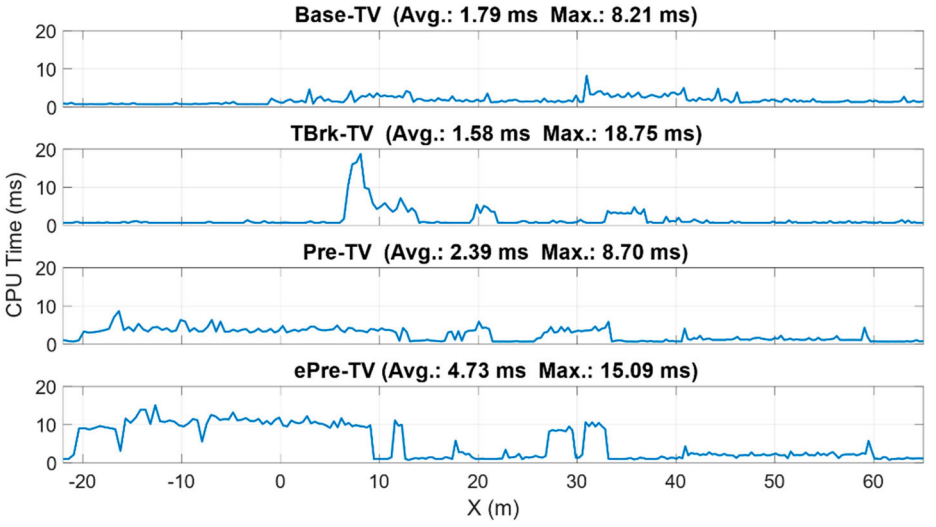

Figure 6. Computational times of the NMPC solution along the obstacle avoidance tests in high tyre-road friction conditions, carried out from the critical speed for the respective vehicle configuration. The titles of the subplots include the average and maximum CPU times along the respective test case.

the CPU time is rather high from $X \approx -20$ m, during the application of the braking control action in straight line, while for TBrk-TV the critical phases are those with maximum curvature, in which trail braking is active. Although ePre–TV implies increased computational load, the CPU times of all controller configurations with the nominal T_s and H_P can be considered rather low. Hence, the algorithms in Figure 6 are deemed appropriate for real time implementation, which has already been achieved for Pre-TV3. On the contrary, Pre-TV2, not included in the figure, experienced higher CPU times by a factor > 15 than Pre-TV, and cannot be considered real time implementable in its current set-up.

Additional simulations demonstrated that the pre-emptive formulation results would further improve with an extension of the prediction horizon. In fact, with long prediction horizons – i.e. corresponding to longer distances than the braking distance to safely bring the vehicle within speeds compatible with the expected course – V_{crit} would almost reach the top speed of the vehicle, provided that the estimate of the expected path ahead is sufficiently accurate. This trend shows that the pre-emptive formulations, differently from Base-TV and TBrk-TV, exploit the potential of the NMPC prediction in full.

Figure 7 reports the results of the obstacle avoidance tests, carried out from the critical speed of the Pre-TV configuration. The Pre-TV and ePre-TV cases are not shown, as they would be almost identical to Figure 4 and well aligned with the reference trajectory. In this case, the Passive configuration becomes unstable and spins in the second part of the manoeuvre. On the contrary, Base-TV stabilises the vehicle, shows significant levels of understeer, and cannot follow the second half of the reference path. The vehicle travels outside the boundaries of the obstacle avoidance course for more than 20 m, which would pose significant safety risks in a real road scenario. The vehicle with the TBrk-TV configuration would hit cones during the initial steering action to avoid the obstacle, and the final steering action to return to the initial lane, although without significantly deviating from the reference course.

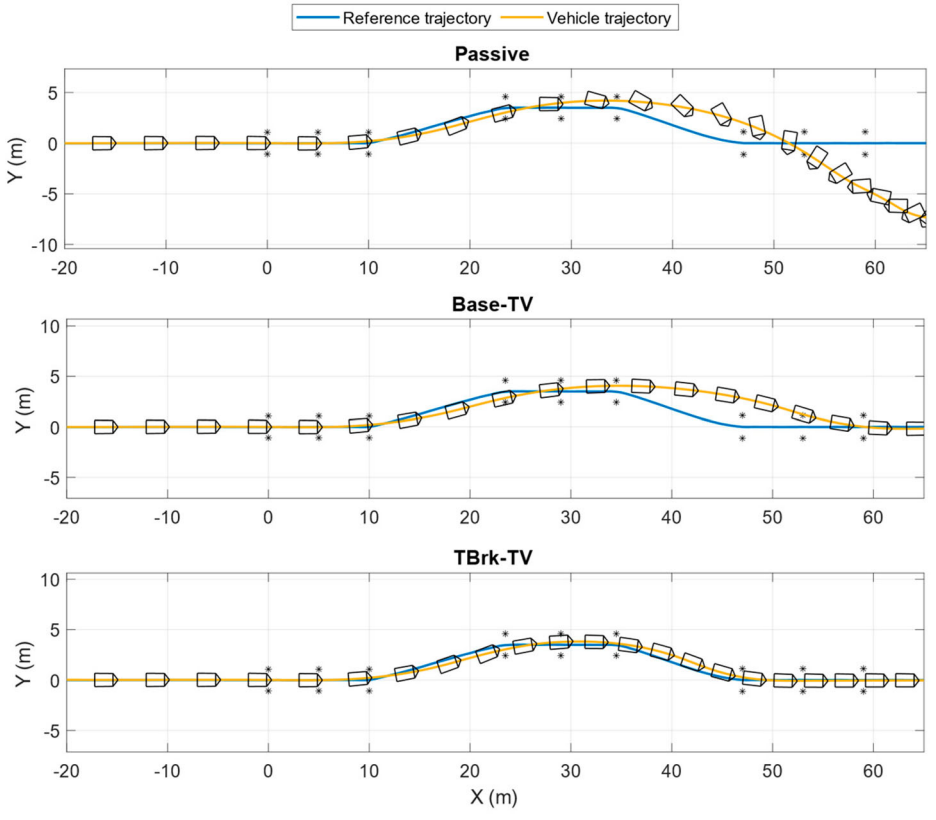

Figure 7. Vehicle trajectories during the obstacle avoidance tests from an initial speed equal to the critical speed of the Pre-TV configuration, in high tyre-road friction conditions.

4.2. Obstacle avoidance in low tyre-road friction conditions

The results of the obstacle avoidance tests in low tyre-road friction conditions, i.e. for a friction parameter equal to 0.6, are reported in Table 3 and Figures 8 and 9. All controller parameters, with the exception of D in (12), which is modified according to the available friction, are unaltered with respect to those in high friction. The results confirm those in Section 4.1, with the following highlights:

- The range of critical speeds is very wide, from $\sim$42 km/h of the Passive vehicle, to $\sim$70 km/h of the ePre-TV, which corresponds to $\sim$25 km/h and $\sim$15 km/h V_{crit} enhancements with respect to Base-TV and TBrk-TV.
- The performances of Base-TV and Base-TV2 in terms of critical and final speeds as well as control effort are substantially undistinguishable, even if Base-TV2 brings less stable vehicle behaviour, with higher $|\alpha_{R,\max}|$.
- Pre-TV2 brings a nearly 3 km/h increase of V_{crit} and a general improvement of the other vehicle dynamics indicators with respect to Pre-TV, although the highest V_{crit} is still achieved by ePre-TV, which also implies a significantly lower CPU time.
- The reduction in the generated direct yaw moment for the cases including trail braking features is clear also in low friction conditions.

Table 3. Key performance indicators along obstacle avoidance tests in low tyre-road friction conditions, carried out from the critical speed for the respective vehicle configuration.

	Passive	Base-TV	Base-TV2	TBrk-TV	Pre-TV	Pre-TV2	Pre-TV3	ePre-TV
V_{crit} (km/h)	41.6	43.6	44.2	54.7	65.8	68.7	65.8	69.5
V_{fin} (km/h)	33.8	32.7	33.3	37.2	36.9	37.0	36.8	35.6
$RMS(e_{\dot{\psi}})$ (deg/s)	4.1	3.6	2.7	2.4	2.0	1.8	2.4	2.1
$\lvert\alpha_{R,\max}\rvert$ (deg)	3.0	1.7	4.0	2.6	2.2	2.0	2.8	1.8
$IA_{\delta_{SW}}$ (deg)	26.0	55.8	53.5	40.5	37.8	33.1	34.0	42.1
$IA_{\Delta\delta_{SW}}$ (deg/s)	108	139	129	128	119	111	117	114
$IA_{\Delta F_x}$ (N)	0	934	957	512	433	512	420	497
$IA_{F_{x\,tot}}$ (N)	0	0	0	174	454	554	460	560

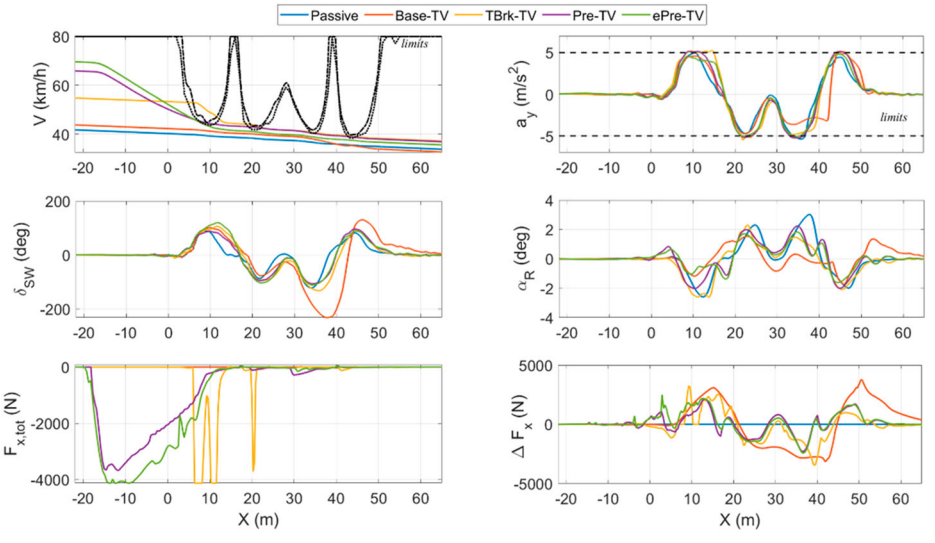

Figure 8. Speed, lateral acceleration, steering wheel angle and rear axle sideslip angle profiles along the obstacle avoidance test in low tyre-road friction conditions, carried out from the critical speed for the respective vehicle configuration. The black dash-dotted and dotted lines in the speed subplot represent the $V_{\max}$ profiles for Pre-TV and ePre-TV.

- Differently from the high tyre-road friction case, in low friction conditions all trail braking formulations provide an increase of the final vehicle speed with respect to the Passive and Base-TV cases.
- The Passive vehicle, which was unstable in the results of Section 4.1 at the critical speed of the Pre-TV case, now significantly understeers, both in the initial and final parts of the obstacle avoidance course, see Figure 9. Hence, in the specific low friction test, the controllers have the main role of increasing agility, rather than stability.
- Agility issues, although attenuated with respect to the Passive case, are also evident in the Base-TV and TBrk-TV set-ups in Figure 9.

In the presented analyses, the tyre-road friction coefficient was supposed to be known, as its estimation is beyond the scope of this work; however, a wide literature is available on the topic, e.g. see [43]. Nevertheless, during the control assessment phase, simulations were run with purposely imposed incorrect values of the tyre-road friction coefficient, e.g.

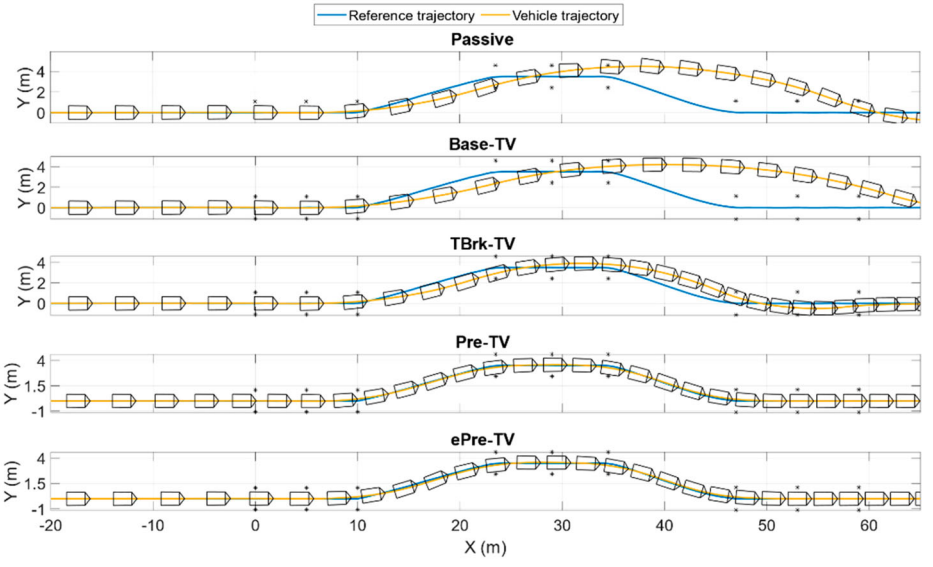

Figure 9. Vehicle trajectories during the obstacle avoidance tests from an initial speed equal to the critical speed of the Pre-TV configuration, in low tyre-road friction conditions.

equal to 0.67 instead of 0.6 (which was the real value), to assess the effect of a reasonable friction estimation tolerance on the performance of the pre-emptive controller. Although the friction condition information is not accurate, the pre-emptive functionalities are still able to slow down the vehicle enough to successfully perform the test from the same or very similar critical speed as the Pre-TV receiving the correct friction information, also thanks to the safety factor included in the formulations.

5. Conclusions

This study presented a new vehicle stability control paradigm, including the pre-emptive application of a trail braking control action. The idea is to keep the vehicle within its stability limits by pre-emptively slowing it down, rather than intervening only after the stability or agility issues are detected. The proposed control function requires: (a) the approximate localisation of the vehicle in the road scenario; and (b) the approximate knowledge of the expected path ahead, for the estimation of the curvature along the prediction horizon.

Two pre-emptive direct yaw moment controllers with different levels of complexity, both of them considering the expected steering angle, reference yaw rate and trajectory radius profiles along the prediction horizon, were implemented and compared with two state-of-the-art non-pre-emptive torque-vectoring controllers excluding and including trail braking, along obstacle avoidance tests at two tyre-road friction levels. All controllers are based on nonlinear model predictive control.

Results show that the formulation without trail braking significantly enhances the vehicle cornering response, but the increase of the maximum successful entry speed of 2–5.5 km/h compared to the passive vehicle is rather small. A considerable improvement is achieved by the non-pre-emptive trail braking formulation, which reaches up to $\sim$ 10 km/h

greater entry speeds, i.e. 62.6 and 54.7 km/h in high and low friction conditions. By far, the most substantial benefit is provided by the pre-emptive formulations, with entry speeds of up to ∼76 km/h and ∼70 km/h for the two tests. This enhancement would undoubtedly have a major impact on the reduction of road accidents in real world scenarios. The analysis of the computational times associated with the pre-emptive controllers shows a rather limited increase of the computational effort, which allows their real time implementation on automotive control hardware.

Future developments will focus on the refinement of the pre-emptive stability control concept, including integration of a wider range of control functions, e.g. the anti-rollover function, electronic brake distribution function, hitch angle control function (to prevent excessive hitch angle oscillations when the controlled vehicle tows a trailer), and wheel slip control function. Also, experimental demonstrations on vehicle prototypes are planned, including separate and integrated implementations of pre-emptive trail braking and torque-vectoring controllers. Moreover, the increase of the technology readiness level of the algorithms will require a systematic study of the functional safety aspects, including formal stability and robustness (e.g. to prevent false activations) analyses.

Disclosure statement

No potential conflict of interest was reported by the author(s).

Funding

This work was supported in part by the Horizon 2020 Framework Programme of the European Commission under grant agreements no. 769944 (STEVE project) and no. 824311 (ACHILES project).

ORCID

Alberto Parra http://orcid.org/0000-0002-3269-214X
Davide Tavernini http://orcid.org/0000-0001-5171-8803
Patrick Gruber http://orcid.org/0000-0003-1030-6655
Aldo Sorniotti http://orcid.org/0000-0002-4848-058X
Asier Zubizarreta http://orcid.org/0000-0001-6049-2308
Joshué Pérez http://orcid.org/0000-0002-0974-5303

References

[1] van Zanten AT, Erhardt R, Pfaff G. VDC, the vehicle dynamics control system of Bosch. SAE Technical Paper 950759, 1995.
[2] van Zanten AT. Bosch ESP systems: 5 years of experience. SAE Technical Paper 2000-01-1633, 2000.
[3] Lie A, Tingvall C, Krafft M, et al. The effectiveness of electronic stability control (ESC) in reducing real life crashes and injuries. Traffic Inj Prev. 2005;7(1):38–43.
[4] Ferguson SA. The effectiveness of electronic stability control in reducing real-world crashes: a literature review. Traffic Inj Prev. 2007;8(4):329–338.
[5] De Novellis L, Sorniotti A, Gruber P, et al. Direct yaw moment control actuated through electric drivetrains and friction brakes: theoretical design and experimental assessment. Mechatronics. 2015;26:1–15.
[6] Esmailzadeh E, Goodarzi A, Vossoughi GR. Optimal yaw moment control law for improved vehicle handling. Mechatronics. 2003;13(7):659–675.

[7] Lu Q, Sorniotti A, Gruber P, et al. H∞ loop shaping for the torque-vectoring control of electric vehicles: theoretical design and experimental assessment. Mechatronics. 2016;35:32–43.
[8] Zhang L, Ding H, Shi J, et al. An adaptive backstepping sliding mode controller to improve vehicle maneuverability and stability via torque vectoring control. IEEE Trans Veh Technol. 2020;69(3):2598–2612.
[9] Goggia T, Sorniotti A, De Novellis L, et al. Integral sliding mode for the torque-vectoring control of fully electric vehicles: theoretical design and experimental assessment. IEEE Trans Veh Technol. 2015;64(5):1701–1715.
[10] Parra A, Zubizarreta A, Perez J, et al. Intelligent torque-vectoring approach for electric vehicles with per-wheel motors. Complexity. 2018: 1–14. doi:10.1155/2018/7030184.
[11] Ataei M, Khajepour A, Jeon S. Model predictive control for integrated lateral stability, traction/braking control, and rollover prevention of electric vehicles. Veh Syst Dyn. 2020;58(1):49–73.
[12] Jalali M, Khosravani S, Khajepour A, et al. Model predictive control of vehicle stability using coordinated active steering and differential brakes. Mechatronics. 2017;48:30–41.
[13] Di Cairano S, Tseng HE, Bernardini D, et al. Vehicle yaw stability control by coordinated active front steering and differential braking in the tire sideslip angles domain. IEEE Trans Control Syst Technol. 2013;21(4):1236–1248.
[14] Wielenga TJ, Chace MA. A method for reducing on-road rollovers - anti-rollover braking. SAE Technical Paper 2000-01-1642, 2000.
[15] Zanchetta M, Tavernini D, Sorniotti A, et al. Trailer control through vehicle yaw moment control: theoretical analysis and experimental assessment. Mechatronics. 2019;64:1–18.
[16] Abroshan M, Hajiloo R, Hashemi E, et al. Model predictive-based tractor-trailer stabilisation using differential braking with experimental verification. Veh Syst Dyn. 2020: 1–24. (in press).
[17] Zarkadis K, Velenis E, Siampis E, et al. Predictive torque vectoring control with active trail-braking. European Control Conference, 2018.
[18] Becker J, Colas MBA, Nordbruch S, et al. Bosch's vision and roadmap toward fully autonomous driving. In: Meyer G, Beiker S, editors. Road vehicle automation. Lecture notes in mobility. Heidelberg: Springer; 2014. p. 49–59.
[19] Funke J, Brown M, Erlien SM, et al. Collision avoidance and stabilization for autonomous vehicles in emergency scenarios. IEEE Trans Control Syst Technol. 2017;25(4):1204–1216.
[20] Falcone P, Tseng HE, Borrelli F, et al. MPC-based yaw and lateral stabilisation via active front steering and braking. Veh Syst Dyn. 2009;46(sup1):611–628.
[21] A. Goodarzi, A. Sabooteh, E. Esmailzadeh, Automatic path control based on integrated steering and external yaw-moment control, Proc Inst Mech Eng, Part K, J Multi-body Dyn. 2008;222(2):189–200.
[22] Chatzikomis C, Sorniotti A, Gruber P, et al. Comparison of path tracking and torque-vectoring controllers for Autonomous electric vehicles. IEEE Trans Intell Veh. 2018;3(4):559–570.
[23] Gao Y, Gordon T. Optimal control of vehicle dynamics for the prevention of road departure on curved roads. IEEE Trans Veh Technol. 2019;68(10):9370–9384.
[24] Grüne L, Pannek J. Nonlinear model predictive control. London: Springer; 2011.
[25] Maciejowski J. Predictive control with constraints. Harlow: Prentice Hall; 2001.
[26] Göhrle C, Wagner A, Schindler A, et al. Active suspension controller using MPC based on a full-car model with preview information, Proceedings of the American Control Conference, pp. 497–502, 2012.
[27] Parra A, Tavernini D, Gruber P, et al. On nonlinear model predictive control for energy-efficient torque-vectoring. IEEE Trans Veh Technol. 2021;70(1):173-188.
[28] Siampis E, Velenis E, Gariuolo S, et al. A real-time nonlinear model predictive control strategy for Stabilization of an electric vehicle at the limits of handling. IEEE Trans Control Syst Technol. 2019;26(6):1982–1994.
[29] Siampis E, Velenis E, Longo S. Rear wheel torque vectoring model predictive control with velocity regulation for electric vehicles. Veh Syst Dyn. 2015;53(11):1555–1579.

[30] Pacejka HB. Tyre and vehicle dynamics. 2nd ed. Oxford: Butterworth-Heinemann; 2006.
[31] Genta A, Genta G. Road vehicle dynamics: fundamentals of modeling and simulation. Singapore: World Scientific; 2016.
[32] Milliken WF, Milliken DL. Race car vehicle dynamics. Warrendale, PA: SAE International1996.
[33] Gillespie TD. Fundamentals of vehicle dynamics. Warrendale, PA: SAE International; 1992.
[34] Parra A, Cagigas D, Zubizarreta A, et al. Modelling and Validation of Full Vehicle Model based on a Novel Multibody Formulation, IECON 2019 - 45th Annual Conference of the IEEE Industrial Electronics Society, 2019.
[35] Dendaluce M, Iglesias I, Martin A, et al. Track testing of a Torque Vectoring Algorithm on a Motor-in-Wheel Car using a Model-Based Methodology with a HiL and Multibody Simulator Setup, International Conference on Intelligent Transportation Systems, 2016.
[36] Cuadrado J, Dopico D, Gonzalez M, et al. A combined penalty and recursive real-time formulation for multibody dynamics. J Mech Des. 2004;126(4):602–608.
[37] Parra A, Rodriguez AJ, Zubizarreta A, et al. Validation of a real-time capable multibody vehicle dynamics formulation for automotive testing frameworks based on simulation. IEEE Access. 2020;8:213253–213265.
[38] Falcone P, Borrelli F, Asgari J, et al. Predictive active steering control for autonomous vehicle systems. IEEE Trans Control Syst Technol. 2007;15(3):566–580.
[39] ISO 3888-2:2011 Passenger cars – Test track for a severe lane-change manoeuvre – Part 2: Obstacle avoidance.
[40] Houska B, Ferreau HJ, Diehl M. An auto-generated real-time iteration algorithm for nonlinear MPC in the microsecond range. Automatica. 2011;47(10):2279–2285.
[41] Quirynen R, Vukov M, Zanon M, et al. Autogenerating microsecond solvers for nonlinear MPC: A tutorial using ACADO integrators. Opt Control Appl and Methods. 2015;36(5):685–704.
[42] Tota A, Lenzo B, Lu Q, et al. On the experimental analysis of integral sliding modes for yaw rate and sideslip control of an electric vehicle with multiple motors. Int J Automot Technol. 2018;19(5):811–823.
[43] Antonov S, Fehn A, Kugi A. Unscented Kalman filter for vehicle state estimation. Veh Syst Dyn. 2011;49(9):1497–1520.